

# Suppression of afterglow in CsI:Tl by codoping with $\text{Eu}^{2+}$ —II: Theoretical model

R.H. Bartram<sup>a</sup>, L.A. Kappers<sup>a</sup>, D.S. Hamilton<sup>a</sup>, A. Lempicki<sup>b</sup>, C. Brecher<sup>b,\*</sup>, J. Glodo<sup>b,c</sup>,  
V. Gaysinskiy<sup>c</sup>, E.E. Ovechkina<sup>c</sup>

<sup>a</sup>Department of Physics, University of Connecticut, Storrs, CT 06269-3046, USA

<sup>b</sup>ALEM Associates, 303A Commonwealth Avenue, Boston, MA 02115, USA

<sup>c</sup>Radiation Monitoring Devices (RMD) Inc., 44 Hunt Street, Watertown, MA 02472, USA

Available online 29 November 2005

## Abstract

The mechanism for afterglow suppression in codoped CsI:Tl,Eu reported in the preceding paper was investigated by combined radioluminescence and thermoluminescence experiments. Model rate equations informed by these experiments were employed to simulate afterglow. It was found that codoping with europium introduces deep electron traps, with room-temperature glow peaks, that effectively scavenge the electrons from shallow traps associated with thallium, thus suppressing afterglow in the time domain of tens of milliseconds.

© 2005 Elsevier B.V. All rights reserved.

PACS: 78.20.Bh; 78.55.–m; 78.55.Fv; 78.60.–b; 78.60.Kn; 78.70.–g

Keywords: Cesium iodide; Radioluminescence; Thermoluminescence; Afterglow model

## 1. Introduction

CsI:Tl is a widely utilized scintillator material with many desirable properties including high density, fast response, high atomic number, high transparency, high radiation resistance, wide availability and low cost. It also has the highest light output of scintillator materials, 64,000 photons/MeV, and is the only material that approaches theoretical efficiency of scintillator response [1]. Unfortunately, its applicability is limited by persistent afterglow at an unacceptably high intensity level. Preliminary experiments have demonstrated the feasibility of ameliorating the deleterious effects of afterglow in CsI:Tl within select time domains by codoping, as reported in the preceding paper [2]. The spectacular success of  $\text{Eu}^{2+}$  in reducing afterglow by a factor of fifty in the millisecond range seems to require a special explanation. The present paper concerns an investigation of codoped CsI:Tl,Eu by radioluminescence and thermoluminescence measurements with low tempera-

ture irradiation. A theoretical model for afterglow suppression is presented, based on the results of this investigation.

## 2. Radioluminescence and thermoluminescence

Radioluminescence and thermoluminescence measurements were performed at the University of Connecticut on a single crystal of codoped CsI:Tl,Eu prepared at RMD with nominally equal concentrations of the two activators, 0.25 mol%. The branching ratio of electron–hole pairs that contribute either to scintillation or thermoluminescence was determined by employing a common apparatus for both measurements [3,4]. An electron Van de Graaff accelerator operated at a beam voltage of 1.0 MeV and a beam current of 1.0  $\mu\text{A}$  was employed as the primary radiation source with the electron beam stopped by a thin copper target that served as a point source of  $\sim 0.5$  MeV gamma rays. The sample was mounted on a heated pedestal monitored by a thermocouple and cooled by flowing nitrogen gas through a heat exchanger. Luminescence was conducted to a photomultiplier by a shielded

\*Corresponding author. Tel.: +617 668 6953; fax: +617 926 9980.

E-mail address: [cbrecher@rmdinc.com](mailto:cbrecher@rmdinc.com) (C. Brecher).

optical fiber. Light outputs for radiation at a nominal temperature of  $-170^{\circ}\text{C}$ , followed by a linear temperature ramp with a nominal ramp rate of  $25^{\circ}\text{C}/\text{min}$ , were recorded for radiation times ranging from 30 s to 16 mins. Light outputs for radiation at  $-170^{\circ}\text{C}$  for times of 8 mins and 16 mins were recorded with a Corning 3-69 filter inserted to block europium recombination luminescence. Light outputs for irradiation at a nominal temperature of  $-60^{\circ}\text{C}$  were also recorded for radiation times ranging from 30 s to 16 mins. Light outputs are plotted as functions of time in Figs. 1, 2 and 3, respectively, for the 16 min irradiation in each case.

### 3. Analysis of glow curves

The thermoluminescence glow curve for CsI:Tl with no Eu shown in Fig. 11 of the preceding paper is reproduced in Fig. 4 for comparison with simulated glow curves.

Three major thermoluminescence glow peaks have been reported previously following irradiation of CsI:Tl at LHT

[5]. The glow peaks at 60, 90 and 120 K have been attributed, respectively, to thermally activated tunneling recombination, the onset of  $V_K$  center mobility, and thermal ionization of electrons from  $\text{TI}^0$  [6,7]. The additional glow peaks at 140 K and 190 K are not intrinsic to CsI:Tl, but may be associated with lattice defects introduced during crystal growth and annealing. In the combined radioluminescence and thermoluminescence experiments, it was expedient to irradiate the CsI:Tl, Eu crystal at a temperature between that of the second and third glow peaks, above the mobility threshold of  $V_K$  centers but low enough to stabilize all of the electron traps. It is evident from the figures that codoping with europium introduces deeper traps with room-temperature glow peaks. Comparison of Figs. 1 and 2 reveals that the activator for these new glow peaks can only be thallium, the same as for the 120 K glow peak, rather than europium; otherwise, the room-temperature glow peaks would be eliminated by the filter. Substitution of a divalent cation

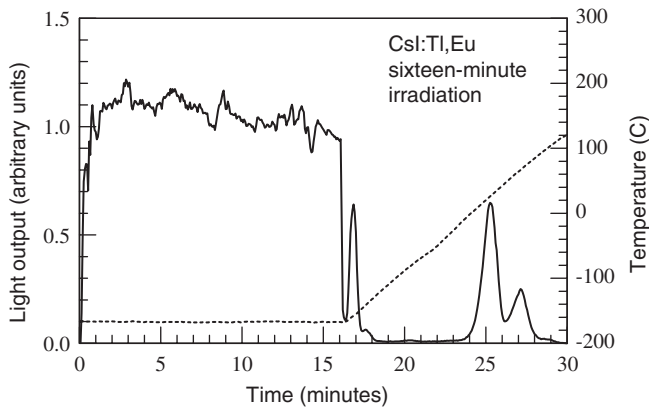


Fig. 1. Recorded light output (continuous curve) and sample temperature (dashed curve) for low temperature ( $-170^{\circ}\text{C}$ ) irradiation of CsI:Tl, Eu with radiation time of 16 mins.

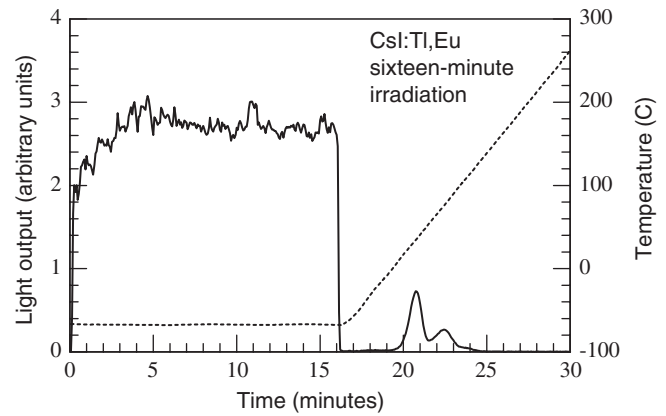


Fig. 3. Recorded light output (continuous curve) and sample temperature (dashed curve) for intermediate-temperature ( $-60^{\circ}\text{C}$ ) irradiation of CsI:Tl, Eu with radiation time of 16 mins.

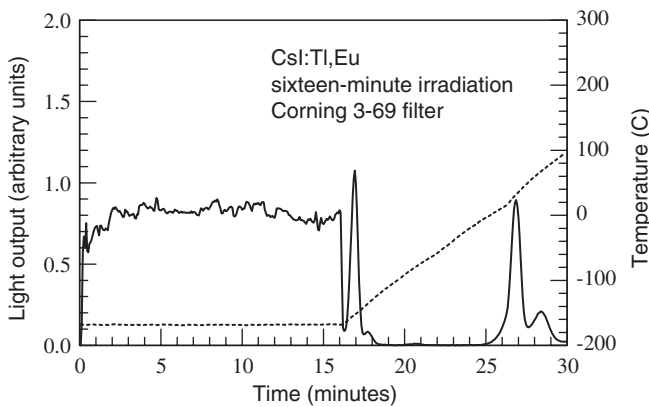


Fig. 2. Recorded light output (continuous curve) and sample temperature (dashed curve) for low temperature ( $-170^{\circ}\text{C}$ ) irradiation of CsI:Tl, Eu with radiation time of 16 min, recorded with a Corning 3-69 filter inserted to block europium recombination luminescence.

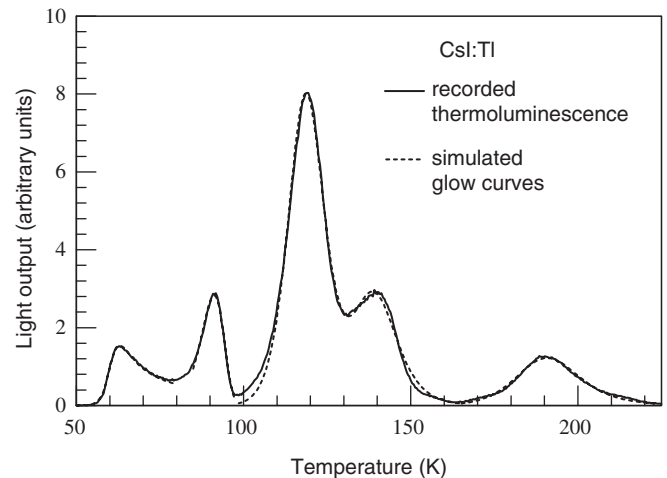


Fig. 4. Glow curve from CsI:Tl single crystal with no  $\text{Eu}^{2+}$  codopant, reproduced from Fig. 11 of Ref. [2], compared with simulation (dashed lines) with the optimized parameter values listed in Table 1.

such as  $\text{Eu}^{2+}$  for the monovalent cation,  $\text{Cs}^+$ , is expected to introduce an electron trap; presumably the extra electron in  $\text{Eu}^+$  is accommodated in a diffuse 6s orbital. Electrons released from both shallow and deep electron traps recombine with holes trapped at thallium ions [ $V_{KA}(\text{Tl}^+)$  centers] before the trapped holes can become mobile. The three successive room-temperature glow peaks are attributed, respectively, to release of electrons from substitutional  $\text{Eu}^+$  ions with charge compensators in nearest-, second-nearest- and third-nearest-neighbor cation sites. A feature of the data revealed by Figs. 1 and 3 is substantial diminution of the quantum efficiency of radioluminescence at temperatures below that of the glow peak at 120 K.

The linear temperature ramp enables interpretation of thermoluminescence glow curves by fitting to explicit solutions [8] of the differential equation

$$\tilde{I} = -\frac{d\tilde{n}}{dt} = \tilde{n}^b p, \quad 1.0 \leq b \leq 2.0 \quad (1)$$

where

$$p(T) = s \exp[-E/k_B T], \quad (2)$$

$$T(t) \equiv T_0 + Rt. \quad (3)$$

First-order kinetics,  $b = 1.0$ , applies in the absence of re-trapping [9,10]. Second-order kinetics,  $b = 2.0$ , prevails when re-trapping predominates [11]. Finally, general-order kinetics,  $1.0 < b < 2.0$ , is a convenient and tractable device for interpolating between first- and second-order kinetics for comparable re-trapping and recombination [12]. The normalized concentration  $\tilde{n}$  in these equations is dimensionless, thus ensuring that the pre-exponential factor  $s$  retains the dimension of reciprocal time even in higher-order kinetics. However, the optimum value of  $s$  for fitting a glow curve is not invariant, but rather depends on the arbitrary choice of normalization constant or, equivalently, on  $\tilde{n}(t_0)$ . An overall scale factor was subsequently applied to fit the measured light output, in order to ensure that absolute values of  $s$  are independent of dose for higher-order kinetics [13]. Simulated glow curves for CsI:Tl with no Eu are compared with recorded thermoluminescence in Fig. 4, and the corresponding optimized parameters are listed in Table 1. The glow curve that peaks at 60 K, attributed to a thermally activated tunneling charge-transfer transition to the emitting state,  $\text{Tl}^0 + V_K \rightarrow \text{Tl}^+ + \text{STE}$ , followed by radiative recombination, cannot

be fitted by a standard glow curve. This glow curve is simulated instead by convolution of a standard glow curve with a tunneling function proportional to inverse time, [14]

$$\tilde{I}(t) = \int_0^t \tilde{I}_{TL}(t') f(t-t') dt', \quad (4)$$

$$f(t) \equiv [\ln(1 + \Delta t/\tau) \times (t + \tau)]^{-1} \theta(\Delta t - t) \quad (5)$$

where  $\theta(t)$  is a unit step function. The standard glow curve  $\tilde{I}_{TL}(t)$  is an explicit solution of Eq. (1) and the convolution of Eq. (4) is evaluated by numerical integration. The parameter  $\tau$  is a measure of the average initial separation of trapped electrons and holes, and  $\Delta t$  is the time required to exhaust them by tunneling recombination, not fully determined by the fitting procedure.

With the observed first-order kinetics of the 90 K glow peak, the lifetime for self-trapping of  $V_K$  centers at room temperature is comparable with the radiative lifetimes of the activators,  $\sim 1 \mu\text{s}$ . Accordingly, self-trapping of  $V_K$  centers makes no significant contribution to room-temperature afterglow on a millisecond time scale.

The glow curves of Fig. 1 following 16 min irradiation of CsI:Tl,Eu are re-plotted in Figs. 5 and 6, together with fitted theoretical glow curves for shallow and deep traps, respectively, with the corresponding optimized parameters listed in Table 2.

#### 4. Rate equations

Additional features of the data can be inferred from postulated model rate equations. It has been established from observation of the asymptotic independence of scintillation rise time on radiation dose rate [15] in the low rate limit that part of the incident energy is transferred

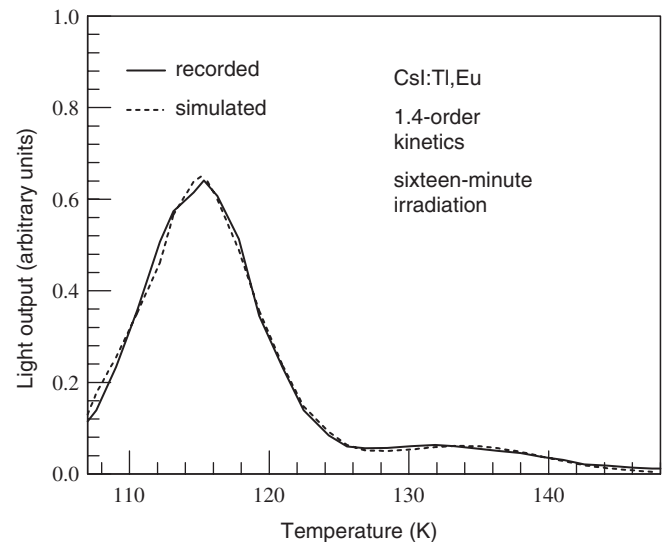


Fig. 5. Low temperature thermoluminescence glow curves of CsI:Tl,Eu (solid line) from Fig. 1 compared with simulation (dashed line) with the optimized parameter values listed in Table 2.

Table 1  
Optimized trap parameters for CsI:Tl inferred from glow curves in Fig. 4

Trap	$T_{\text{peak}}$ (K)	$b$	$E$ (eV)	$s$ ( $10^{14} \text{ min}^{-1}$ )	$\tilde{n}(t_0)$	$\tau$ (min)
$\text{Tl}^0 + V_K$	60	1.9	0.20423	9187.75	1.0	0.45780
$V_K$	90	1.0	0.19926	0.00273	1.0	–
Tl(1)	120	1.9	0.31005	0.52860	0.58816	–
Tl(2)	140	1.9	0.34757	0.23413	0.25184	–
Tl(3)	190	2.0	0.46082	0.12946	0.16000	–

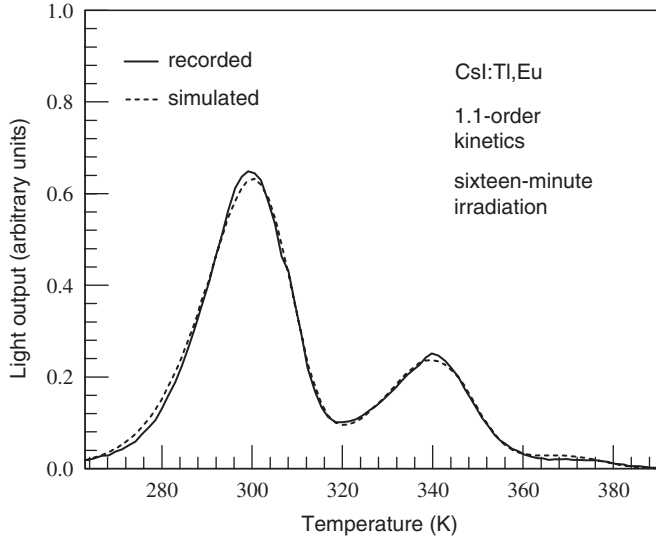


Fig. 6. Room-temperature thermoluminescence glow curves of CsI:TI,Eu (solid line) from Fig. 1 compared with simulation (dashed line) with the optimized parameter values listed in Table 2.

Table 2  
Optimized trap parameters for CsI:TI,Eu inferred from glow curves in Figs. 5 and 6

Trap	$T_{\text{peak}}$ (K)	$b$	$E$ (eV)	$s$ ( $10^{14} \text{ min}^{-1}$ )	$\tilde{n}(t_0)$
TI(1)	120	1.4	0.31199	1.20469	0.24990
TI(2)	140	1.4	0.34114	0.46115	0.02975
Eu(1)	300	1.1	0.86934	1.33143	0.48278
Eu(2)	340	1.1	0.95794	0.58290	0.20958
Eu(3)	370	1.1	1.04067	0.63581	0.02799

directly to excitons rather than to independent electrons and holes. Accordingly, the concentration  $f$  of electron–hole pairs generated per unit time can be represented as

$$f = f_x + f_r \quad (6)$$

where  $f_x$  is the exciton component and  $f_r$  is the component of free electrons and holes. The reduction in quantum efficiency at low temperature is attributed to nonradiative recombination of self-trapped excitons. Rate equations that incorporate these observations are as follows:

$$\frac{dn_c}{dt} = f_r - n_c n_h A_{\text{rch}} - n_c \sum_i N_e^{(i)} A_e^{(i)} + \sum_i n_e^{(i)} p_e^{(i)}, \quad (7a)$$

$$\frac{dn_v}{dt} = f_r - n_v \sum_i n_e^{(i)} A_{\text{rve}}^{(i)} - n_v N_h A_h, \quad (7b)$$

$$\frac{dn_e^{(i)}}{dt} = n_c \sum_i N_e^{(i)} A_e^{(i)} - n_v \sum_i n_e^{(i)} A_{\text{rve}}^{(i)} - n_e^{(i)} p_e^{(i)}, \quad (7c)$$

$$\frac{dn_h}{dt} = n_v N_h A_h - n_c n_h A_{\text{rch}}, \quad (7d)$$

$$\frac{dn_x}{dt} = f_x - n_x \sum_i N_x^{(i)} A_x^{(i)} - n_x A_{\text{rx}}(T), \quad (7e)$$

$$\sum_i \frac{dn_a^{(i)}}{dt} = n_c n_h A_{\text{rch}} + n_v \sum_i n_e^{(i)} A_{\text{rve}}^{(i)} - \sum_i n_a^{(i)} [\tau_r^{(i)}]^{-1} + n_x \sum_i N_x^{(i)} A_x^{(i)}, \quad (7f)$$

$$I = \sum_i n_a^{(i)} [\tau_r^{(i)}]^{-1} \quad (7g)$$

where  $n_c$  is the concentration of conduction electrons,  $n_v$  that of itinerant holes ( $V_K$  centers);  $n_e^{(i)}$  those of trapped electrons;  $n_h$  that of holes trapped near  $\text{TI}^+$  ions [ $V_{KA}(\text{TI}^+)$  centers];  $n_x$  that of mobile excitons;  $n_a^{(i)}$  those of excited activators of the  $i$ th type;  $N_e^{(i)}$  those of electron traps of the  $i$ th type; and  $N_h$  those of hole traps. Trap concentrations are implicitly assumed to be much larger than the concentrations of trapped charges; their apparent saturation is a reflection of dynamic equilibrium. Thermal ionization rates are defined by

$$p_e^{(i)} = s_e^{(i)} \exp[-E_e^{(i)}/k_B T]. \quad (8)$$

Charge conservation is implicit in Eqs. (7),

$$\frac{dn_c}{dt} + \sum_i \frac{dn_e^{(i)}}{dt} = \frac{dn_v}{dt} + \frac{dn_h}{dt} \quad (9)$$

and with the further assumption of no pre-existing trapped charges, Eq. (9) implies

$$n_c + \sum_i n_e^{(i)} = n_v + n_h. \quad (10)$$

Since Eqs. (7) involve too many independent parameters to be tractable, model rate equations are adopted for illustrative purposes that incorporate the following simplifying assumptions and approximations:

$$n_e^{(i)}, n_h \gg n_c, n_v, n_x, n_a^{(i)}, \quad (11a)$$

$$\frac{dn_c}{dt}, \frac{dn_v}{dt}, \frac{dn_x}{dt}, \frac{dn_a^{(i)}}{dt} \cong 0, \quad (11b)$$

$$A_{\text{rch}} \cong A_{\text{rve}}^{(i)} \equiv A_r, \quad (11c)$$

$$\sum_i N_e^{(i)} A_e^{(i)} = N_h A_h. \quad (11d)$$

It follows from Eqs. (10) and (11a) that

$$\sum_i n_e^{(i)} \cong n_h. \quad (12)$$

One can then eliminate the smaller concentrations and the rate equations reduce to

$$\frac{d\tilde{n}_e^{(i)}}{dt} \cong \frac{\tilde{f}_r + \sum_i \tilde{n}_e^{(i)} p_e^{(i)}}{(1 + \tilde{n}_h)} \delta^{(i)} - \tilde{n}_e^{(i)} \left[ p_e^{(i)} + \frac{\tilde{f}_r}{1 + \tilde{n}_h} \right], \quad (13a)$$

$$\frac{d\tilde{n}_h}{dt} \cong \frac{\tilde{f}_r(1 - \tilde{n}_h) - \tilde{n}_h \sum_i \tilde{n}_e^{(i)} p_e^{(i)}}{(1 + \tilde{n}_h)}, \quad (13b)$$

$$\tilde{I} = Q\tilde{f}_x + \tilde{f}_r - \frac{d\tilde{n}_h}{dt} \cong Q\tilde{f}_x + \frac{2\tilde{f}_r\tilde{n}_h + \tilde{n}_h \sum_i \tilde{n}_e^{(i)} p_e^{(i)}}{(1 + \tilde{n}_h)} \quad (13c)$$

where

$$\tilde{n}_e^{(i)} \equiv n_e^{(i)}/n_f, \quad (14a)$$

$$\tilde{f} \equiv f/n_f, \quad (14b)$$

$$\tilde{I} \equiv I/n_f, \quad (14c)$$

$$n_f \equiv N_h A_h / A_r, \quad (14d)$$

$$\delta^{(i)} \equiv \frac{N_e^{(i)} A_e^{(i)}}{N_h A_h}, \quad \sum_i \delta^{(i)} = 1, \quad (14e)$$

$$Q(T) \equiv \sum_i N_x^{(i)} A_x^{(i)} / A_{nrx}(T). \quad (14f)$$

Eqs. (13) neglect transients on a time scale of microseconds.

## 5. Low-temperature irradiation

Several parameters remain unspecified in Eqs. (13). To determine their values, the integrated scintillation light output  $S$  and integrated thermoluminescence light output  $G$  of CsI:TI,Eu were calculated as functions of radiation time from low temperature radioluminescence and thermoluminescence data. The quantity  $(G+S)/t$ , plotted in Fig. 7 as a function of radiation time at  $-170^\circ\text{C}$ , is seen to be essentially constant as expected, since Eq. (13c) predicts the proportionality

$$(G+S)/t \propto Q(T)f_x + f_r. \quad (15)$$

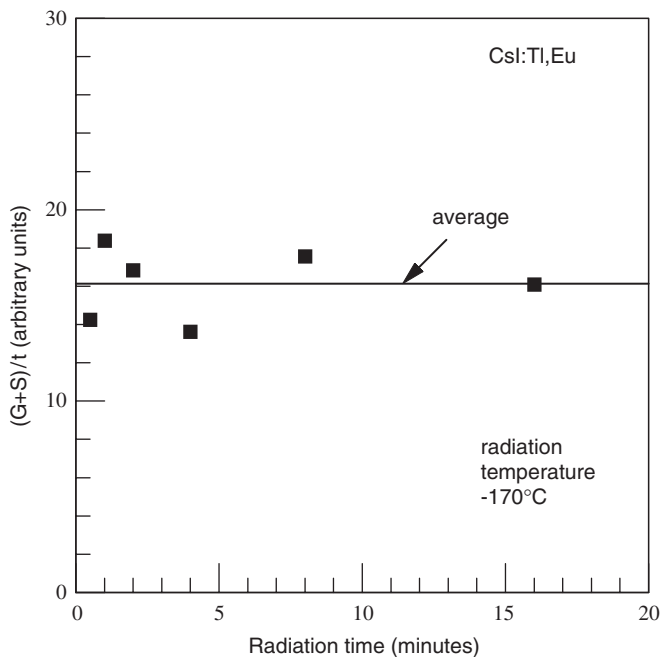


Fig. 7. Total integrated light output of CsI:TI,Eu divided by radiation time,  $(G+S)/t$  (solid squares), as a function of radiation time at  $-170^\circ\text{C}$ .

This observation confirms that the reduction of quantum efficiency is associated only with the exciton component as assumed, since only scintillation should be affected by it. Presumably, the threshold for exciton mobility is comparable to that for  $V_K$  center mobility, but just above the threshold temperature most excitons move too slowly to reach  $\text{TI}^+$  ions before decaying nonradiatively.

Since the thermal ionization rates  $p_e^{(i)}$  are negligible at  $-170^\circ\text{C}$  for the traps of interest, Eqs. (13a) and (13b) are reduced, respectively, to

$$\frac{d\tilde{n}_e^{(i)}}{dt} \cong \frac{\tilde{f}_r(\delta^{(i)} - \tilde{n}_e^{(i)})}{(1 + \tilde{n}_h)}, \quad (16a)$$

$$\frac{d\tilde{n}_h}{dt} \cong \frac{\tilde{f}_r(1 - \tilde{n}_h)}{(1 + \tilde{n}_h)} \quad (16b)$$

with solutions

$$\tilde{f}_r t = -\tilde{n}_h - 2 \ln(1 - \tilde{n}_h), \quad (17a)$$

$$\tilde{n}_e^{(i)} = \delta^{(i)} \tilde{n}_h. \quad (17b)$$

The quantity  $G/G_{\text{max}}$  is plotted in Fig. 8 as a function of radiation time at  $-170^\circ\text{C}$ , where it is compared with  $\tilde{n}_h(t)$  from Eq. (17a) with the fitted parameter value  $\tilde{f}_r = 0.625$ , listed in Table 3.

The quantity  $G/S$  is plotted in Fig. 9 as a function of radiation time at  $-170^\circ\text{C}$ , where it is compared with the

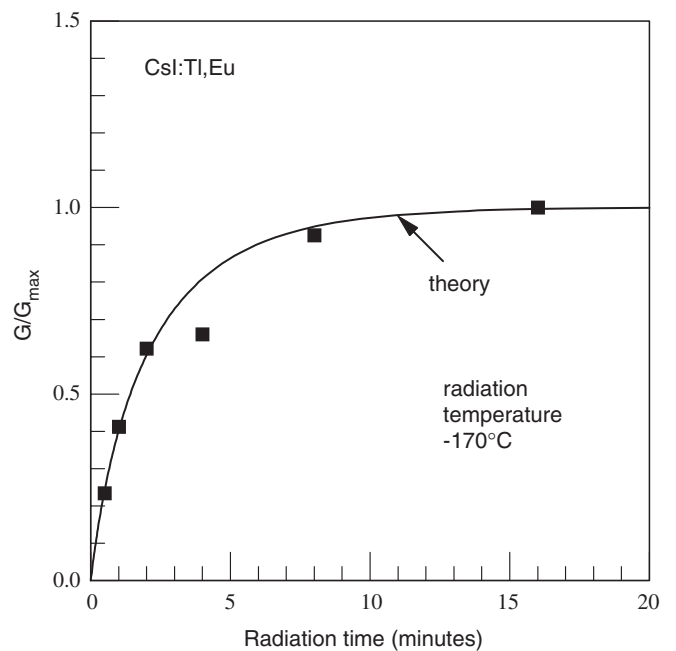


Fig. 8. Integrated thermoluminescence light output of CsI:TI,Eu,  $G/G_{\text{max}}$  (solid squares), as a function of radiation time at  $-170^\circ\text{C}$ , compared with the theoretical trapped-hole concentration  $\tilde{n}_h$  from Eq. (17a) with  $\tilde{f}_r = 0.625$  (continuous curve).

Table 3

Comparison of parameter values inferred from low and intermediate temperature data

Parameter\Rad. Temp.	−170 °C	−60 °C
$\tilde{f}_r$	0.625	0.45
$Q(T)/R$	0.47	(2.7) <sup>a</sup>
$R \equiv \tilde{f}_r/\tilde{f}_x$	(0.37) <sup>a</sup>	0.37
$Q(T)$	0.17	1.0

<sup>a</sup>Assumed values.

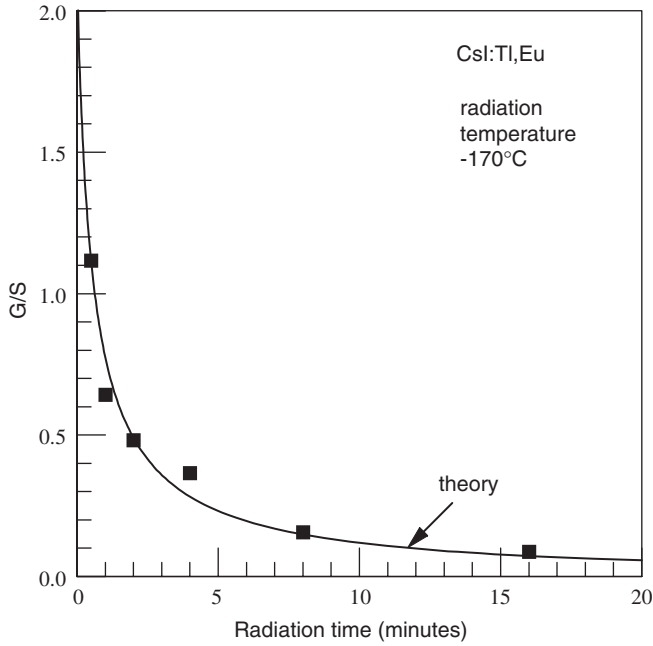


Fig. 9. Ratio of integrated thermoluminescence light output to integrated scintillation light output of CsI:Tl,Eu,  $G/S$  (solid squares), as a function of radiation time at  $-170^\circ\text{C}$ , compared with the theoretical prediction from Eq. (18) with  $Q(T)/R = 0.47$  (continuous curve).

theoretical expression

$$\frac{G}{S} = \frac{\tilde{n}_h}{[Q(T)\tilde{f}_x + \tilde{f}_r]t - \tilde{n}_h} = \frac{\tilde{n}_h}{Q(T)\tilde{f}_x t - 2[\tilde{n}_h + \ln(1 - \tilde{n}_h)]} \quad (18)$$

with the fitted parameter value,  $Q(T)\tilde{f}_x/\tilde{f}_r \equiv Q(T)/R = 0.47$ , listed in Table 3.

### 6. Intermediate temperature irradiation

In order to evaluate the parameters  $Q(T)$  and  $R \equiv \tilde{f}_r/\tilde{f}_x$  independently, the integrated scintillation light output  $S$  and integrated thermoluminescence light output  $G$  of CsI:Tl,Eu were calculated as functions of radiation time from intermediate temperature ( $-60^\circ\text{C}$ ) radioluminescence and thermoluminescence data as well. By virtue of the large number of distinguishable glow peaks and their depen-

dence on the dopant concentration, it is expedient to simplify the rate equations further for higher temperature applications by retaining only two types of electron trap in codoped CsI:Tl,Eu and only one type in singly doped CsI:Tl. Since the  $\text{Tl}^0$  and  $\text{Eu}^+$  centers in CsI:Tl,Eu contribute almost equally to  $G$ , it is assumed for the codoped material that

$$\delta^{(\text{Tl})} = \delta^{(\text{Eu})} = 1/2. \quad (19)$$

Eqs. (13a) and (13b) can be specialized to CsI:Tl,Eu and to the radiation phase at  $-60^\circ\text{C}$  by retaining  $p_e^{(\text{Tl})}$  and neglecting  $p_e^{(\text{Eu})}$ ,

$$\frac{d\tilde{n}_e^{(\text{Tl})}}{dt} \cong \frac{\tilde{f}_r + \tilde{n}_e^{(\text{Tl})}p_e^{(\text{Tl})}}{2(1 + \tilde{n}_h)} - \tilde{n}_e^{(\text{Tl})}p_e^{(\text{Tl})} \cong 0, \quad (20a)$$

$$\frac{d\tilde{n}_h}{dt} \cong \frac{\tilde{f}_r(1 - \tilde{n}_h) - \tilde{n}_h\tilde{n}_e^{(\text{Tl})}p_e^{(\text{Tl})}}{(1 + \tilde{n}_h)} \quad (20b)$$

and combined to yield

$$\frac{d\tilde{n}_h}{dt} \cong \tilde{f}_r \left[ \frac{(1 - 2\tilde{n}_h^2)}{(1 + 3\tilde{n}_h + 2\tilde{n}_h^2)} \right] \quad (21)$$

with solution

$$\tilde{f}_r t = -\tilde{n}_h + \sqrt{2} \tanh^{-1}(\tilde{n}_h\sqrt{2}) - \frac{3}{4} \ln(1 - 2\tilde{n}_h^2). \quad (22)$$

The quantity  $(G + S)/t$  as a function of radiation time at  $-60^\circ\text{C}$  was found to be essentially constant as well. The integrated thermoluminescence light output,  $G/G_{\text{max}}$ , plotted as a function of radiation time at  $-60^\circ\text{C}$  in Fig. 10, is compared with the corresponding theoretical

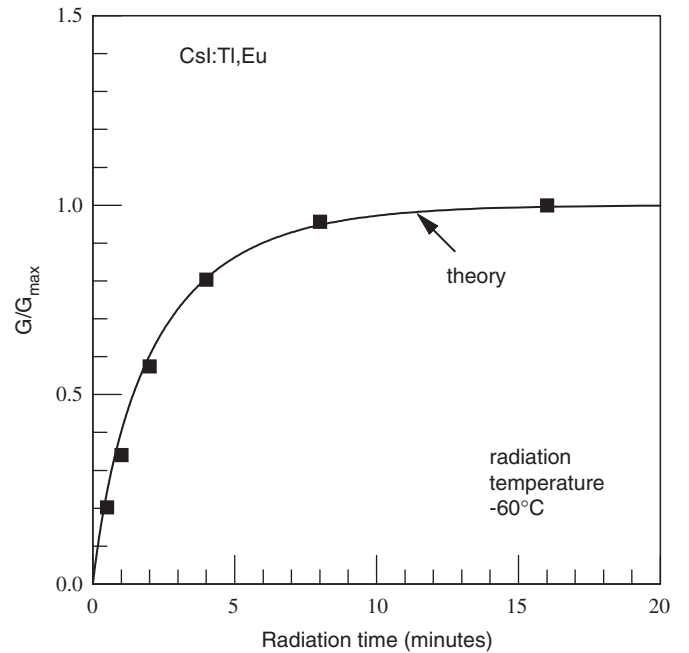


Fig. 10. Integrated thermoluminescence light output of CsI:Tl,Eu,  $G/G_{\text{max}}$  (solid squares), as a function of radiation time at  $-60^\circ\text{C}$ , compared with the theoretical prediction from Eqs. (22) and (23) with  $\tilde{f}_r = 0.45$  (continuous curve).

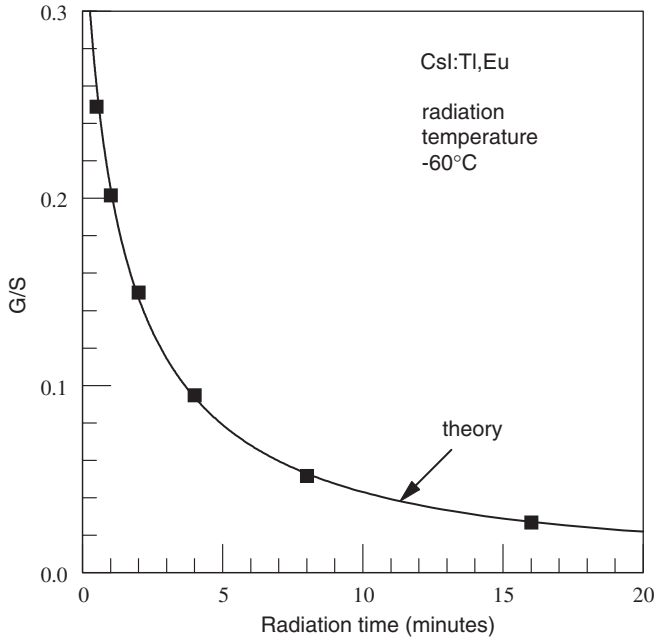


Fig. 11. Ratio of integrated thermoluminescence light output to integrated scintillation light output of CsI:Tl,Eu,  $G/S$  (solid squares), as a function of radiation time at  $-60^\circ\text{C}$ , compared with theoretical prediction from Eq. (24) with  $R \cong \tilde{f}_r/\tilde{f}_x \cong 0.37$  (continuous curve).

function,

$$(G/G_{\max})_{\text{theory}} = \sqrt{2\tilde{n}_h(t)} \quad (23)$$

with the optimized parameter value  $\tilde{f}_r = 0.45$ , also listed in Table 3.

The ratio  $G/S$ , plotted as a function of radiation time at  $-60^\circ\text{C}$  in Fig. 11, is compared with the theoretical expression

$$\left(\frac{G}{S}\right)_{\text{theory}} = \frac{\tilde{n}_h}{(\tilde{f}_x + \tilde{f}_r)t - \tilde{n}_h} \quad (24)$$

with the optimized parameter value,  $R \equiv \tilde{f}_r/\tilde{f}_x \cong 0.37$ , listed in Table 3.

The parameter values inferred from the present light output data, recorded for irradiation at  $-60^\circ\text{C}$ , are compared in Table 3 with those inferred from data recorded for irradiation at  $-170^\circ\text{C}$ . The scintillation light output varies with temperature in proportion to  $[Q(T) + R]$  and thus increases by a factor of 2.5 between  $-170^\circ\text{C}$  and  $-60^\circ\text{C}$ .

## 7. Rate equations for thermoluminescence

It is instructive to specialize the postulated rate equations for CsI:Tl,Eu to the thermoluminescence phase. The rate equations can be further specialized to low temperature,  $p_e^{(\text{Eu})} \cong 0$ , and to room temperature,  $\tilde{n}_e^{(\text{Tl})}$ ,  $d\tilde{n}_e^{(\text{Tl})}/dt \cong 0$ . The relevant low-temperature rate equation is

$$\tilde{I} = -\frac{d\tilde{n}_h}{dt} \cong \frac{\tilde{n}_h \tilde{n}_e^{(\text{Tl})} p_e^{(\text{Tl})}}{(1 + \tilde{n}_h)} \quad (25)$$

and the relevant room temperature rate equation is

$$\tilde{I} = -\frac{d\tilde{n}_h}{dt} \cong \frac{2\tilde{n}_h^2 p_e^{(\text{Eu})}}{(1 + 2\tilde{n}_h)}. \quad (26)$$

The nearly first-order kinetics of the room temperature glow curve shown in Fig. 6 is clearly inconsistent with Eq. (26). The inconsistency can be resolved by postulating that the cross-section for electron trapping by  $\text{Eu}^{2+}$  is negligible in the absence of ionizing radiation,  $A_e^{(\text{Eu})} \cong 0$ . Eqs. (25) and (26) are then replaced, respectively, by

$$\tilde{I} = -\frac{d\tilde{n}_h}{dt} \cong \frac{2\tilde{n}_h \tilde{n}_e^{(\text{Tl})} p_e^{(\text{Tl})}}{(1 + 2\tilde{n}_h)} \quad (27)$$

and

$$\tilde{I} = -\frac{d\tilde{n}_h}{dt} \cong \tilde{n}_h p_e^{(\text{Eu})}. \quad (28)$$

Eq. (27) is consistent with general-order kinetics, and Eq. (28) with first-order kinetics.

## 8. Room temperature irradiation

The following inequalities apply for codoped CsI:Tl,Eu in the room-temperature radiation phase:

$$\tilde{n}_e^{(\text{Tl})} p_e^{(\text{Tl})} \gg \tilde{n}_e^{(\text{Eu})} p_e^{(\text{Eu})}, \quad (29a)$$

$$\tilde{n}_e^{(\text{Tl})} \ll \tilde{n}_e^{(\text{Eu})}. \quad (29b)$$

Of particular interest in the present application is the limit of short radiation time,  $\tilde{f}_r t_{\text{rad}} \ll 1$ . In this limit, one obtains the approximate rate equations

$$\frac{d\tilde{n}_e^{(\text{Tl})}}{dt} \cong \frac{\tilde{f}_r - \tilde{n}_e^{(\text{Tl})} p_e^{(\text{Tl})} + \tilde{n}_e^{(\text{Eu})} p_e^{(\text{Eu})}}{2} \cong 0, \quad (30a)$$

$$\frac{d\tilde{n}_e^{(\text{Eu})}}{dt} \cong \frac{\tilde{f}_r + \tilde{n}_e^{(\text{Tl})} p_e^{(\text{Tl})} - \tilde{n}_e^{(\text{Eu})} p_e^{(\text{Eu})}}{2}, \quad (30b)$$

$$\frac{d\tilde{n}_h}{dt} \cong \tilde{f}_r \quad (30c)$$

with solutions

$$\tilde{n}_h \cong \tilde{n}_e^{(\text{Eu})} \cong \tilde{f}_r t_{\text{rad}}, \quad (31)$$

$$\tilde{n}_e^{(\text{Tl})} \cong \tilde{f}_r / p_e^{(\text{Tl})}, \quad (32)$$

$$\tilde{I}(t_{\text{rad}}) = \tilde{f}_x + \tilde{f}_r - \frac{d\tilde{n}_h}{dt} \cong \tilde{f}_x. \quad (33)$$

## 9. Afterglow

The approximate rate equations for codoped CsI:Tl,Eu in the afterglow phase in the limit of short radiation time are

$$\frac{d\tilde{n}_e^{(\text{Tl})}}{dt} \cong -2\tilde{n}_h \tilde{n}_e^{(\text{Tl})} p_e^{(\text{Tl})} + \tilde{n}_e^{(\text{Eu})} p_e^{(\text{Eu})}, \quad (34a)$$

$$\frac{d\tilde{n}_e^{(\text{Eu})}}{dt} \cong -\tilde{n}_e^{(\text{Eu})}p_e^{(\text{Eu})}, \quad (34b)$$

$$\frac{d\tilde{n}_h}{dt} \cong -2\tilde{n}_h\tilde{n}_e^{(\text{Tl})}p_e^{(\text{Tl})}. \quad (34c)$$

These equations involve two very different time scales. An approximate solution is

$$\tilde{n}_e^{(\text{Tl})} \cong \left[ \frac{\tilde{f}_r}{p_e^{(\text{Tl})}} - \frac{p_e^{(\text{Eu})}}{2p_e^{(\text{Tl})}} \right] \exp(-2\tilde{f}_r t_{\text{rad}} p_e^{(\text{Tl})} t) + \frac{p_e^{(\text{Eu})}}{2p_e^{(\text{Tl})}}, \quad (35a)$$

$$\tilde{n}_e^{(\text{Eu})} \cong \tilde{f}_r t_{\text{rad}} \exp(-p_e^{(\text{Eu})} t), \quad (35b)$$

$$\begin{aligned} \frac{\tilde{I}(t)}{\tilde{I}(0)} &\cong -\frac{1}{\tilde{f}_x} \frac{d\tilde{n}_h}{dt} = -\frac{1}{\tilde{f}_x} \left( \frac{d\tilde{n}_e^{(\text{Tl})}}{dt} + \frac{d\tilde{n}_e^{(\text{Eu})}}{dt} \right) \\ &\cong R t_{\text{rad}} [(2\tilde{f}_r - p_e^{(\text{Eu})}) \exp(-2\tilde{f}_r t_{\text{rad}} p_e^{(\text{Tl})} t) \\ &\quad + p_e^{(\text{Eu})} \exp(-p_e^{(\text{Eu})} t)]. \end{aligned} \quad (36)$$

In the absence of the europium codopant, Eq. (14e) implies  $\delta^{(\text{Tl})} = 1$  and Eq. (13a) for the radiation phase is reduced to

$$\frac{d\tilde{n}_h}{dt} \cong \frac{\tilde{f}_r(1 - \tilde{n}_h) - \tilde{n}_h^2 p_e^{(\text{Tl})}}{(1 + \tilde{n}_h)}. \quad (37)$$

Since  $p_e^{(\text{Tl})}$  is so large at room temperature, the trapped hole concentration  $\tilde{n}_h$  quickly reaches its saturation value,

$$\tilde{n}_h \cong \sqrt{\frac{\tilde{f}_r}{p_e^{(\text{Tl})}}} \ll 1.0 \quad (38)$$

with saturation light output

$$\tilde{I} = \tilde{f}_x + \tilde{f}_r. \quad (39)$$

The corresponding equation for the afterglow phase is then reduced to

$$\frac{d\tilde{n}_h}{dt} \cong -\tilde{n}_h^2 p_e^{(\text{Tl})} \quad (40)$$

with solution

$$\tilde{n}_h \cong \sqrt{\frac{\tilde{f}_r}{p_e^{(\text{Tl})}} \left( \frac{t_{0e}}{t_{0e} + t} \right)}, \quad (41a)$$

$$t_{0e} \equiv \frac{1}{\sqrt{p_e^{(\text{Tl})} \tilde{f}_r}}, \quad (41b)$$

$$\frac{\tilde{I}(t)}{\tilde{I}(0)} \cong -\left( \frac{1}{\tilde{f}_x + \tilde{f}_r} \right) \left( \frac{d\tilde{n}_h}{dt} \right) \cong \left( \frac{R}{1 + R} \right) \left( \frac{t_{0e}}{t_{0e} + t} \right)^2. \quad (42)$$

Afterglow simulations based on Eq. (36) for codoped CsI:Tl,Eu and on Eq. (42) for singly doped CsI:Tl, with parameter values from Tables 1–3, are plotted in Fig. 12 for comparison with Figs. 6 and 7 of the preceding paper.

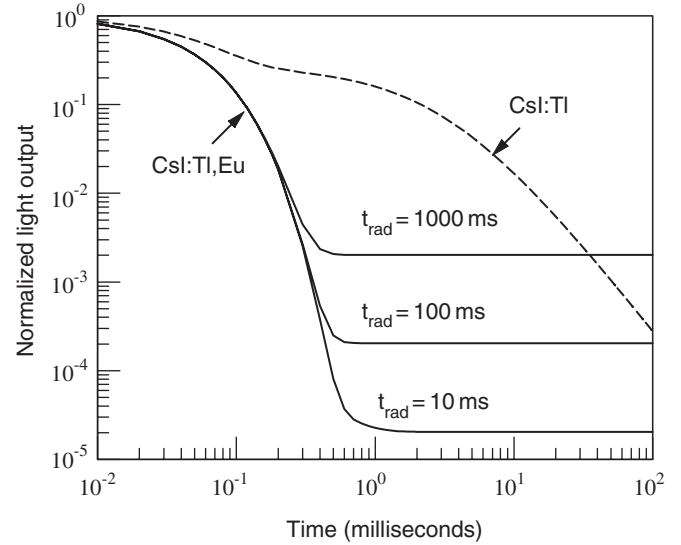


Fig. 12. Log-log plot of simulated afterglow of codoped CsI:Tl,Eu for several radiation times from Eq. (36), compared with simulated afterglow of singly doped CsI:Tl from Eq. (42), with  $\tilde{f}_r = 1.0$ ,  $R = 0.37$ , and the parameter values listed in Table 1 for Tl(1) and in Table 2 for Tl(1) and Eu(1). Decay of scintillation light output of the form  $\exp(-qt)$ ,  $q = 20 \text{ ms}^{-1}$ , simulates the fall time of the radiation source.

## 10. Time-resolved spectra

The time-resolved spectra displayed in Figs. 9 and 10 of the preceding paper require special consideration because the time scale involved is too short to be compatible with approximations adopted to simplify the rate equations. CsI:Tl, with cesium chloride structure, differs from thallium-activated alkali halides with rock-salt structure in that  $\text{Tl}^{2+}$  is not stable [16]. Accordingly, the recombination mechanism is somewhat different in this material. The two lower-energy emission bands at 2.55 and 2.25 eV have been ascribed to self-trapped excitons perturbed by  $\text{Tl}^+$  in first and second neighbor positions, respectively [17]. However, an experiment on CsI:Tl conducted with low temperature X-ray excitation [18] and discriminating multiple resonance techniques [19] suggests a donor–acceptor transition in which the emitting state is better described as  $\text{Tl}^0$  perturbed by a  $V_K$  center ( $\text{Tl}^0 + V_K$ ) rather than a self-trapped exciton perturbed by a  $\text{Tl}^+$  ion ( $\text{Tl}^+ + \text{STE}$ ). These competing interpretations can be reconciled by invoking an intervening tunneling charge transfer transition in the recombination process. In the majority of cases at room temperature, excitons migrate to activators where they are trapped to establish the emitting state ( $\text{Tl}^+ + \text{STE}$ ). In the remaining cases, conduction electrons are trapped at activators, while the corresponding holes are self-trapped on the anion sub-lattice as  $V_K$  centers. A  $V_K$  center then diffuses to the vicinity of a neutral activator ( $\text{Tl}^0$ ) where recombination occurs by a two-step process involving a tunneling charge-transfer transition to the emitting state, ( $\text{Tl}^0 + V_K \rightarrow \text{Tl}^+ + \text{STE}$ ), followed by radiative recombination.

Ionized activators ( $\text{Tl}^+$ ) foster afterglow by impeding diffusion of  $V_K$  centers, forming  $V_{KA}(\text{Tl}^+)$  centers that are stable for minutes at room temperature. Following irradiation, electrons thermally ionized from  $\text{Tl}^0$  are trapped at the  $\text{Tl}^+$  ion component of the  $V_{KA}(\text{Tl}^+)$  center, forming a  $(\text{Tl}^0 + V_K)$  center that subsequently recombines by the two-step tunneling and radiative recombination process described above, leaving behind isolated  $\text{Tl}^+$ . (Although isolated  $\text{Tl}^0$  is thermally ionized in less than a microsecond at room temperature,  $\text{Tl}^0$  stabilized by a neighboring  $V_K$  center can persist long enough for tunneling to occur.) However, it should be recognized that the designation  $V_{KA}(\text{Tl}^+)$  does not describe a single entity, but rather a class of point defects in which the  $V_K$  center component can assume a variety of positions with respect to the  $\text{Tl}^+$  ion component [20]. It has been shown that the tunneling probability is acutely sensitive to the separation of the two components, and that tunneling contributes time dependence proportional to  $t^{-1}$  to the afterglow [21]. The progressive red shift as a function of time delay following the X-ray pulse that is evident in the time-resolved spectra of CsI:Tl shown in Fig. 9 of the preceding paper is then attributed to sequential tunneling in  $(\text{Tl}^0 + V_K)$  centers with  $\text{Tl}^0$  in first and second neighbor positions with respect to the  $V_K$  center. Subsequent sequential radiative recombination of the resulting STEs perturbed by  $\text{Tl}^+$  in first and second neighbor positions produces the emission bands at 2.55 and 2.25 eV, respectively, with a superposition of the two bands at intermediate times. Note that this room-temperature tunneling between first and second neighbors occurs on a much shorter time scale than the long range tunneling involved in the 60 K glow peak. Time resolved spectra of codoped CsI:Tl, Eu following short-pulse irradiation shown in Fig. 10 of the preceding paper [2] reveal that radiative recombination of excitons with  $\text{Eu}^{2+}$  ions or of  $V_K$  centers with  $\text{Eu}^+$  ions to produce europium emission is a transient phenomenon that persists only for tens of microseconds until the populations of itinerant excitons and  $V_K$  centers are depleted.

## 11. Summary and conclusions

It had been established in prior investigations of CsI:Tl that  $\text{Tl}^+$  activators serve both as shallow electron traps and as deep hole traps, and that afterglow in this material may be attributed to thermal ionization of trapped electrons ( $\text{Tl}^0$ ) followed by radiative recombination with trapped holes [ $V_{KA}(\text{Tl}^+)$ ]. Reduction of the total integrated thermoluminescence light output  $G$  with increasing Eu concentration in Fig. 11 of the preceding paper suggests that the concentration of hole traps is diminished by codoping, perhaps by partial charge compensation of  $\text{Eu}^{2+}$  with  $\text{Tl}^0$ , but that effect is not sufficient to explain the observed afterglow suppression. It is evident from the radioluminescence and thermoluminescence light-output data presented here that codoping of CsI:Tl with  $\text{Eu}^{2+}$  introduces additional deep electron

traps. Although both  $\text{Tl}^+$  and  $\text{Eu}^{2+}$  activators are involved in scintillation, it was established that only  $\text{Tl}^+$  activators participate in thermoluminescence; accordingly, room-temperature glow peaks may be attributed to thermal ionization of trapped electrons from  $\text{Eu}^+$ , followed by radiative recombination with trapped holes [ $V_{KA}(\text{Tl}^+)$ ]. Application of postulated rate equations to light-output data reveals that a substantial fraction of the absorbed energy is transferred to the activators by excitons, thus bypassing both electron and hole traps, and that the exciton component is strongly quenched at low temperature. It is also inferred from thermoluminescence glow curves that the cross-section for electron trapping by  $\text{Eu}^{2+}$  is negligible in the absence of ionizing radiation.

A mathematical model for afterglow suppression in co-doped CsI:Tl, Eu predicts that the deep electron traps introduced by codoping with europium effectively scavenge the electrons from shallow traps associated with thallium, thus suppressing afterglow in the time domain of tens of milliseconds. However, the ultimate release of electrons trapped by europium contributes to enhanced afterglow in the longer time domain of seconds and minutes, unlike the analogous mechanism in codoped  $(\text{Y, Gd})_2\text{O}_3:\text{Eu, Pr}$  [22], where deferred recombination is nonradiative. Trapping of holes to form stable  $V_{KA}(\text{Tl}^+)$  centers is common to both CsI:Tl and CsI:Tl, Eu and is ultimately responsible for their afterglow. Since most of the energy is transported to activators during radioluminescence by excitons that bypass both electron and hole traps, the scintillation light output is nearly independent of radiation time as indicated in Eq. (31), even though the traps are far from saturated. For the same reason, Eq. (36) predicts that the long-time component of afterglow is proportional to radiation time but independent of radiation intensity, consistent with Figs. 6 and 7 in the preceding paper. It is evident from Fig. 12 that afterglow simulations based on the present model bear at least a qualitative resemblance to recorded afterglow as displayed in these figures.

## Acknowledgments

We thank the Public Health Service (NIH), DHHS for Grants R44-EB003382-01 and -02, and the Medical Sciences Div., DoE, for Grant DE-FG01-03ER83760, which provided partial support for parts of this work.

## References

- [1] R.H. Bartram, A. Lempicki, J. Lumin. 68 (1996) 225.
- [2] C. Brecher, A. Lempicki, S.R. Miller, E.E. Ovechkina, V. Gaysinskiy, V.V. Nagarkar, R.H. Bartram, Suppression of afterglow in CsI:Tl by codoping with  $\text{Eu}^{2+}$  I. Experimental (preceding paper, this issue).
- [3] R.H. Bartram, D.S. Hamilton, L.A. Kappers, A. Lempicki, J. Lumin. 75 (1997) 183.
- [4] R.H. Bartram, A. Lempicki, L.A. Kappers, D.S. Hamilton, J. Lumin. 106 (2004) 169.

- [5] V. Babin, K. Kalder, A. Krasnikov, S. Zazubovich, J. Lumin. 96 (2002) 75.
- [6] T. Sidler, J.P. Pellaux, A. Nouailhat, M.A. Aegerter, Solid State Commun. 13 (1973) 479.
- [7] M. Barland, E. Duval, A. Nouailhat, J. Phys. C 14 (1981) 4237.
- [8] R. Chen, S.W.S. McKeever, Theory of Thermoluminescence and Related Phenomena, World Scientific, Singapore, 1997.
- [9] J.T. Randall, M.H.F. Wilkins, Proc. R. Soc. A 184 (1945) 365.
- [10] J.T. Randall, M.H.F. Wilkins, Proc. R. Soc. A 184 (1945) 390.
- [11] G.F.J. Garlick, A.F. Gibson, Proc. Phys. Soc. 60 (1948) 574.
- [12] C.E. May, J.A. Partridge, J. Chem. Phys. 40 (1964) 1401.
- [13] M.S. Rasheedy, J. Phys.: Condens. Matter 5 (1993) 633.
- [14] C.J. Delbecq, Y. Toyozawa, P.H. Yuster, Phys. Rev. B 9 (1974) 4497.
- [15] S. Chernov, J. Lumin. 72–74 (1997) 751.
- [16] P.A. Rodnyi, Physical Processes in Inorganic Scintillators, CRC Press, Boca Raton, New York, 1997.
- [17] V. Nagirnyi, A. Stolovich, S. Zazubovich, V. Zepelin, E. Mihokova, M. Nikl, G.P. Pazzi, L. Salvini, J. Phys.: Condens. Matter 7 (1995) 3637.
- [18] J.-M. Spaeth, W. Meise, K.S. Song, J. Phys.: Condens. Matter 6 (1994) 3999.
- [19] J.-M. Spaeth, J.R. Niklas, R.H. Bartram, Structural Analysis of Point Defects in Solids, Springer, Berlin, Heidelberg, 1992.
- [20] V. Babin, K. Kalder, A. Krasnikov, S. Zazubovich, J. Lumin. 96 (2002) 75.
- [21] C.J. Delbecq, Y. Toyozawa, P.H. Yuster, Phys. Rev. B 9 (1974) 4497.
- [22] W. Köstler, A. Winnacker, W. Rossner, B.C. Grabmaier, J. Phys. Chem. Solids 56 (1995) 907.